D. J. Smith and J. R. Gordon†*

Application of Elastic–Plastic Defect Assessments to a Flawed Carbon–Manganese Steel Pressure Vessel

REFERENCE Smith, D. J. and Gordon, J. R., **Application of elastic–plastic defect assessments to a flawed carbon–manganese steel pressure vessel**, *Defect Assessment in Components – Fundamentals and Applications*, ESIS/EGF9 (Edited by J. G. Blauel and K.-H. Schwalbe) 1991, Mechanical Engineering Publications, London, pp. 1005–1023.

ABSTRACT The CEGB structural assessment procedure R6, revision 3, and The Welding Institute proposed revisions to BSI, PD6493, crack tip opening displacement (CTOD) methods for fracture assessments have been used to predict the fracture behaviour of a large-scale pressure vessel containing a through-thickness longitudinal defect. Conditions for ductile crack initiation and fracture instability have been evaluated and are compared with experimental results.

The deformation and fracture of the vessel was more complex than expected. It was found that there were higher than predicted hoop stresses. There were also tensile residual stresses. Using measured rather than predicted stresses gave experimental points outside the FAD assessment lines for both assessment routes and for ductile initiation and fracture instability. The predicted initiation pressure from the R6 route was higher than obtained experimentally using predicted hoop stresses. Although final failure was brittle, the assessment routes gave lower failure pressures for ductile failure than was observed. Because of the uncertainty in the prediction of the stresses, together with the treatment of residual stresses, the safety factor 2 in level 1 of the proposed PD6493 may be justified.

Introduction

Welded structures are often found to contain defects and, depending on the type of the applied loading, these defects could grow to the point where failure of the structure can occur. Considerable work has been undertaken to provide a means of assessing the significance of defects with regard to structural integrity. In particular, recent advances in elastic–plastic fracture mechanics have prompted revisions to the fracture assessment procedures used by the CEGB and The Welding Institute. The overall objective of the project was to critically investigate the ability of the current fracture assessment procedures to predict the behaviour of a large-scale pressure vessel containing a defect. It should be noted, however, that this is different to the usual use of structural integrity assessment routes, which are meant to define the conditions to avoid premature failure.

The most common fracture assessment procedure for general welded structures is the CTOD design curve approach **(1)** which forms the basis of the elastic–plastic fracture assessment procedure in BSI PD6493 : 1980. This approach, however, has a number of drawbacks **(2)** and attempts have been

* Department of Mechanical Engineering, University of Bristol, BS8 1TR, UK.
† Edison Welding Institute, 1100 Kinnear Road, Columbus, Ohio 43212, USA.

made to develop assessment procedures which are more accurate than the current CTOD design curve. This has resulted in proposed changes to the CTOD fracture assessment methods given in PD6493 : 1980. The proposals include the incorporation of a CTOD plastic collapse modified strip yield model **(3)** and a CTOD reference stress model **(4)**. Further modifications to these models have been proposed by Gordon and Garwood **(2)**.

The CEGB structural assessment procedure **(5)** has also recently been revised **(6)** to account for the strain hardening capacity of high work hardening materials, by altering the shape of the failure assessment diagram (FAD). There has also been a change in the normalisation parameter used on the abscissa of such diagrams to a yield based parameter, rather than the collapse based parameter used previously **(5)**.

In this paper, the CEGB and The Welding Institute fracture assessment procedures are used to predict the behaviour of a large-scale pressure vessel containing a defect. A brief outline of the test programme is given below. Further details can be found in references **(7)** and **(8)**. The fracture assessments are then applied, and the results are critically assessed.

Test programme

The material selected for the test programme was a BS1501-151 Grade 430A carbon manganese steel supplied as a 25 mm thick plate 1 m by 1 m square. The chemical composition is shown in Table 1. The plate was hot rolled to the correct curvature and thickness suitable for welding into a pressure vessel. Two panels were extracted from the plate; one panel 400 mm wide by 400 mm long was extracted for welding into a pressure vessel and the other panel was removed for material characterisation tests. The former panel was machined to a thickness of 22 mm to match the wall thickness of the pressure vessel.

The pressure vessel consisted of a seam welded 22 mm thick, 870 mm inner diameter, 3 m length of API 5LX56 pipe material. The end caps of the vessel were two hemispherical pieces formed from 38 mm thick BS4360 Grade 50D steel. In order to perform the test on the BS1501-151 Grade 430A material, a panel of material 400 mm by 400 mm was removed from the mid-section of the pipe.

The carbon manganese steel panel was welded into the vessel using a preheat of 100°C, a MIG root run and an MMA fill using Fortrex 7018 electrodes. On completion of welding, the panel was subjected to a heat treatment of 150°C for 12 hours to minimise problems of hydrogen cracking. The vessel

Table 1 Chemical composition: percentage by weight

C	*Mn*	*Si*	*S*	*P*	*Cu*
0.11	1.32	0.35	0.01	0.016	0.25

Plus traces of Cr and Mo

was strain-gauged internally and externally using biaxial and rosette gauges. The wiring for internal strain gauges was let out through a nozzle in one end cap, as shown in Fig. 1.

Centre hole surface residual stress measurements **(9)** were made in the region of the panel to be notched, both on the inside and the outside surfaces of the panel. The average residual stress in the hoop direction, $\sigma_{\theta,r}$, was determined to be about 55 MPa **(7)(8)**. Because of the nature of the welded panel in the pressure vessel, it is not clear whether the residual stresses represent long or short range stresses. This is considered in the next section. A through-thickness longitudinal notch, 67 mm long, was then machined into the panel. In order to prevent leakage at the notch during testing, a layer of neoprene rubber was applied to the inner surface and backed by a steel shim. This covering was liberally coated with mastic and stainless steel foil spot-welded around the outside.

Displacement transducers and cantilever clip gauges were placed in the vicinity of the notch. To monitor crack growth, an AC PD system was used,

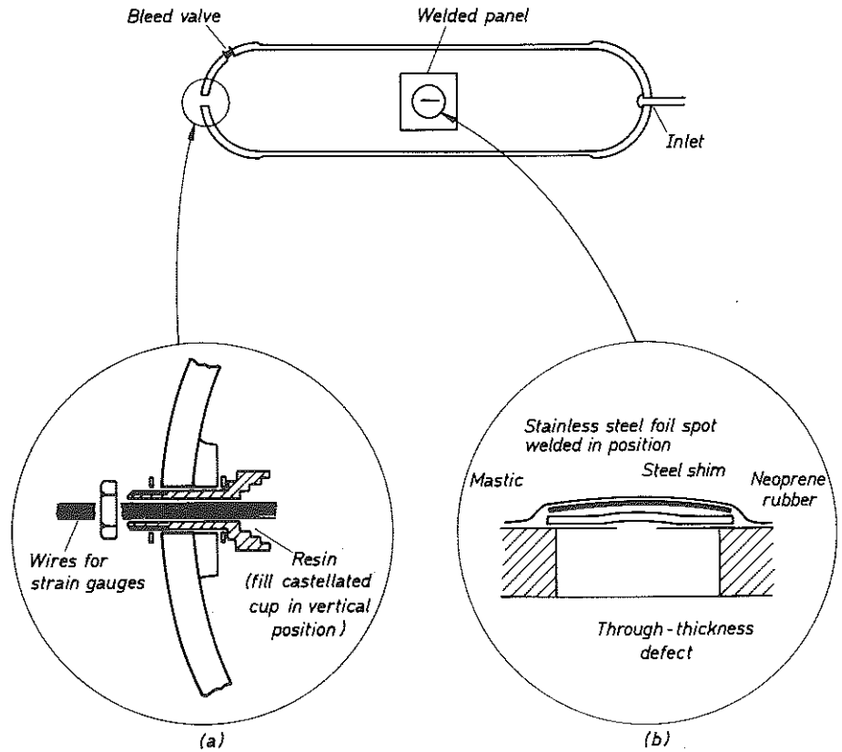

Fig 1 Schematic diagram of the pressure vessel construction
(a) leak-proof fitting for the strain gauge wires
(b) sealing arrangement on the inside surface over the notch

with current input and voltage output monitoring leads positioned close to the notch. To sharpen the tips of the notch, the vessel was pressure cycled to produce fatigue crack growth of about 2–3 mm at each notch tip.

After pre-cracking, the vessel was pressurised slowly to 11.7 MPa, at which point the pump tripped out. The vessel was re-pressurised to 14.7 MPa. After this pressurisation, visual inspection of the external surface of the vessel revealed approximately 2 mm of ductile crack extension at the two notch tips. The vessel was re-pressurised to produce further crack growth and sudden failure took place at 162. MPa. The clip gauge response is shown in Fig. 2.

Subsequent observation of the fracture faces revealed that initiation was ductile and significant crack tunnelling had taken place. Final fracture occurred from a cleavage crack initiating at the end of the ductile tear.

From the internal and external strain gauge rosettes, the internal and external wall surface hoop stresses have been determined. The stresses, as a function of applied pressure, p, are shown in Fig. 3. Also shown, is the mean

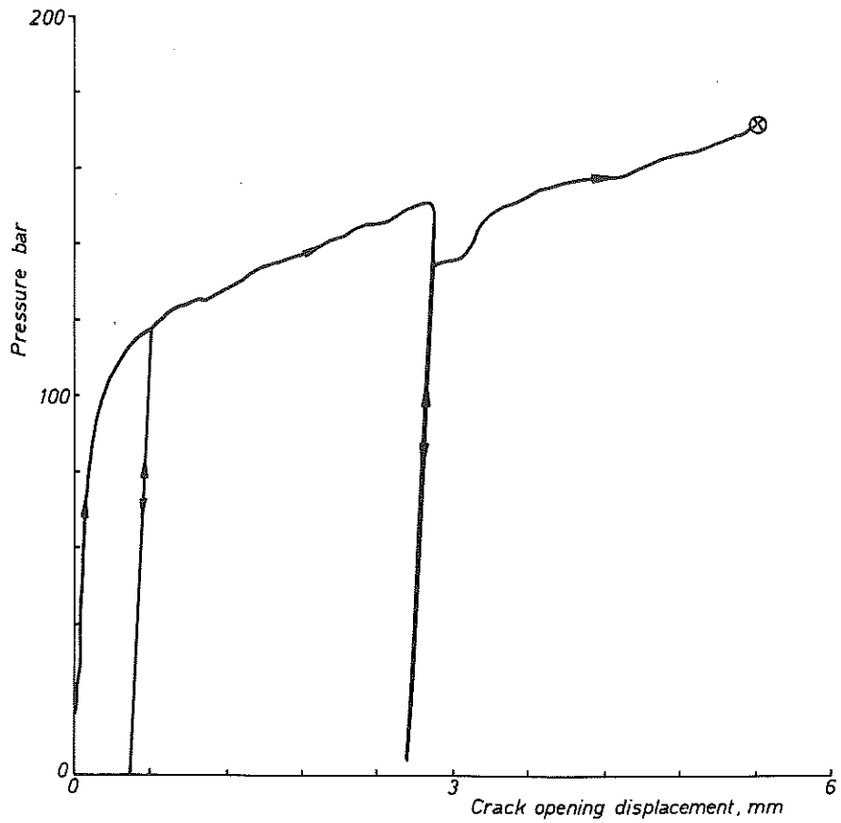

Fig 2 Pressure vessel response during pressurisation

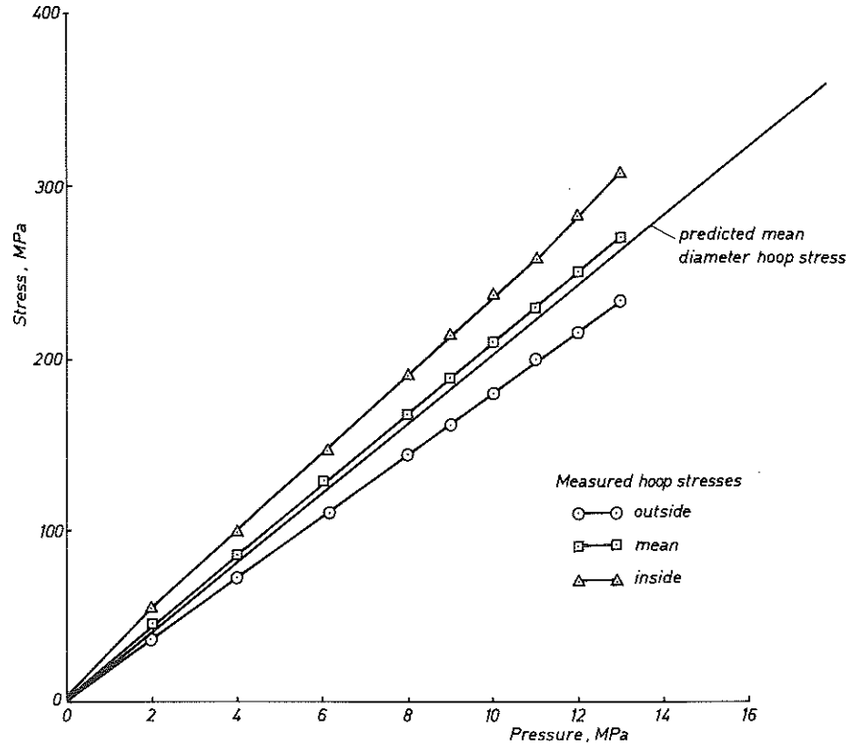

Fig 3 Measured and calculated hoop stresses

diameter hoop stress given by

$$\sigma_{\theta,\mathrm{p}} = p\,\frac{R_\mathrm{m}}{t} \tag{1}$$

where R_m is the mean radius and t is the wall thickness. It can be seen from Fig. 3 that, while the experimental mean hoop stress was reasonably close to the predicted stress, the hoop stresses on the inner wall surface were significantly higher than anticipated. This has considerable bearing on the fracture predictions given in the next section.

It was certain that the final failure pressure was 16.2 MPa. However, it was not immediately evident at which pressure crack initiation took place. When the test was interrupted at 14.7 MPa, it was observed that approximately 2 mm of ductile tearing had taken place on the surface. Subsequent observation of the final fracture surfaces indicated that at 14.7 MPa the crack had tunnelled and the maximum extent of ductile tearing was about 9.5 mm. Crack initiation had therefore occurred significantly before 14.7 MPa. Subsequent

Table 2 Tensile data for C–Mn steel

σ_{nom} MPa	ε_{nom}	σ_{true} MPa	ε_{true}
309	0.0027	310	0.0027
310	0.0039	312	0.0039
310	0.0139	315	0.0138
329	0.0164	335	0.0163
342	0.0202	349	0.0199
373	0.0291	383	0.0287
404	0.0404	420	0.0396
435	0.0567	459	0.0551
466	0.0841	505	0.0807
497	0.1465	569	0.1367

analysis of the local deformation and the ACPD voltage suggested that initiation may have taken place at a pressure as low as 11 MPa. This pressure is used in the subsequent analyses for initiation. Details of the analysis leading to the choice of the initiation pressure are given in references **(7)** and **(8)**.

In addition to the pressure vessel test, tensile and ductile crack growth tests were carried out using specimens extracted from the second panel described earlier. The calculated true stress as a function of true plastic strain, obtained from the tensile tests, is shown in Table 2. The yield and ultimate strengths for the carbon manganese steel are 310 and 500 MPa respectively.

Measurements of crack tip opening displacement (CTOD) and J were obtained from sidegrooved compact tension (CT) and single edge notch bend (SENB) specimens using established in-house procedures **(10)(11)**. Further details of the ductile crack growth tests, and the results obtained, can be found in references **(7)** and **(8)**.

Fracture assessments

The detail of the various assessments can be found elsewhere **(6)(12)**. Here, the essential outline and necessary equations are presented without their derivation.

CEGB R6 (revision 3) assessments (6)

R6 (revision 3) gives three options for the failure assessment diagram (FAD) used in any analysis, namely: Option 1 – a lower bound FAD for use in the absence of any material properties; Option 2 – a FAD derived from tensile data for the material; and Option 3 – a FAD based on a J integral analysis of the specimen geometry. Since a J integral analysis is not known for the pressure vessel, Option 3 is not considered in the present study.

Within each option, R6 (revision 3) recommends three levels of analysis based on the crack growth allowed in the structure, namely: Category 1 – based on initiation of crack growth, at which the material toughness $J_{0.2}$ corresponds to 0.2 mm of crack growth; Category 2 – the material toughness J_g is

restricted to the limit of valid crack growth resistance data; and Category 3 – based on material toughness data beyond the limits of J validity.

In the following, attention is directed specifically to Categories 1 and 3 to predict initiation and fracture instability respectively. For both categories, a lower bound R curve is used. For category 1, $J_{0.2} = 125$ kJ/m^2 and, for category 3, the full resistance curve up to 12 mm of crack growth is used.

The normalised toughness parameter K_r is separated into two components K_r^p and K_r^s where

$$K_r = K_r^p + K_r^s \tag{2}$$

K_r^p is the normalised toughness parameter for primary loads such as applied mechanical and other system stresses, such as long range residual stresses, given by

$$K_r^p = K_I^p / K_{mat} \tag{3}$$

where K_I^p is the stress intensity factor for the primary loads and K_{mat} is the material toughness obtained from

$$K_{mat} = \sqrt{\{EJ_{mat}/(1 - \nu^2)\}} \tag{4}$$

where J_{mat} is the measured toughness, as defined by the various categories of analysis described above. The Young's modulus, E, was assumed to be 207 GPa.

K_r^s is the normalised toughness parameter for secondary loads such as short range welding residual stresses, given by

$$K_r^s = \frac{K_I^s}{K_{mat}} + \rho \tag{5}$$

K_I^s is the stress intensity factor for the secondary loads. The correction factor ρ takes account of the plasticity interaction effects between secondary and primary stresses.

The stress intensity factor K_I for a through-thickness longitudinal crack in a pressure vessel is given by

$$K_I = \sigma_\theta M \sqrt{(\pi a)} \tag{6}$$

where σ_θ is the applied $\sigma_{\theta,p}$ or the residual hoop stress $\sigma_{\theta,r}$ and M is the Folias correction factor **(14)** to take account of bulging of the cylinder given by

$$M = \frac{4 - k}{2}\left(1 + 1.622\,\frac{a^2}{Rt}\right)^{1/2} \tag{7}$$

where

$$k = \begin{cases} 3 - 4\nu & \text{plane strain} \\ (3 - \nu)/(1 + \nu) & \text{plane stress} \end{cases} \tag{8}$$

The normalised load parameter L_r is defined as the ratio of the total applied load giving rise to the σ^p stresses to the load at which yielding takes place.

As pointed out earlier, the residual stresses for the notched welded panel in the pressure vessel may be treated as either long-range or short-range stresses. For the former case, the residual stresses are equivalent to primary stresses, in which case the normalised load parameter L_r is given by

$$L_r = \frac{\sigma_\theta M}{\sigma_Y} \tag{9}$$

where σ_θ is the sum of the hoop stress from pressure loading $\sigma_{\theta,p}$ and the residual stresses $\sigma_{\theta,r}$. If the residual stresses are treated as short-range, σ_θ is obtained from pressure loading alone, $\sigma_{\theta,p}$.

In the following, the Folias correction factor M, equation (7) is evaluated for plane strain conditions and $\nu = 0.3$. The factor M is strictly applicable only to the elastic régime. Once yielding and subsequent deformation has taken place, the correction due to bulging in elastic–plastic conditions is not known. However, in this instance, M is applied for all crack lengths regardless of the extent of deformation.

Option 1 – FAD

The relationship between K_r and L_r for the FAD is given by

$$K_r = (1 - 0.14L_r^2)\{0.3 + 0.7 \exp(-0.65L_r^6)\} \tag{10}$$

$$L_r \leqslant L_r^{max} \tag{11}$$

where L_r^{max} is the ratio of the flow strength σ_f to the yield strength σ_Y. The flow strength is the average of the yield and ultimate strengths. Equation (10) is shown in Fig. 4.

Option 2 – FAD

The relationship between K_r and L_r for the Option 2 FAD is given by

$$K_r = \left(\frac{E\varepsilon_R}{L_r\sigma_Y} + \tfrac{1}{2}L_r^3\sigma_Y/E\varepsilon_R\right)^{-1/2} \tag{12}$$

$$L_r \leqslant L_r^{max} \tag{13}$$

where ε_R is the reference strain at the reference stress σ_R equal to $L_r\sigma_Y$ on the true stress–strain curve.

The Option 2 FAD is plotted in Fig. 4.

Conventionally, the failure assessment diagrams provide a means of defining the conditions for avoiding premature failure. For initiation conditions, the prediction points for the Option 1 and 2 FAD are shown in Fig. 4(a). The line representing the locus of points $[K_r : L_r]$ for increasing pressure for zero residual stress starts at the origin and intersects the Option 1 and 2 FAD lines at the same $[K_r : L_r]$ point. The points $[K_r : L_r]$ have been evaluated using the

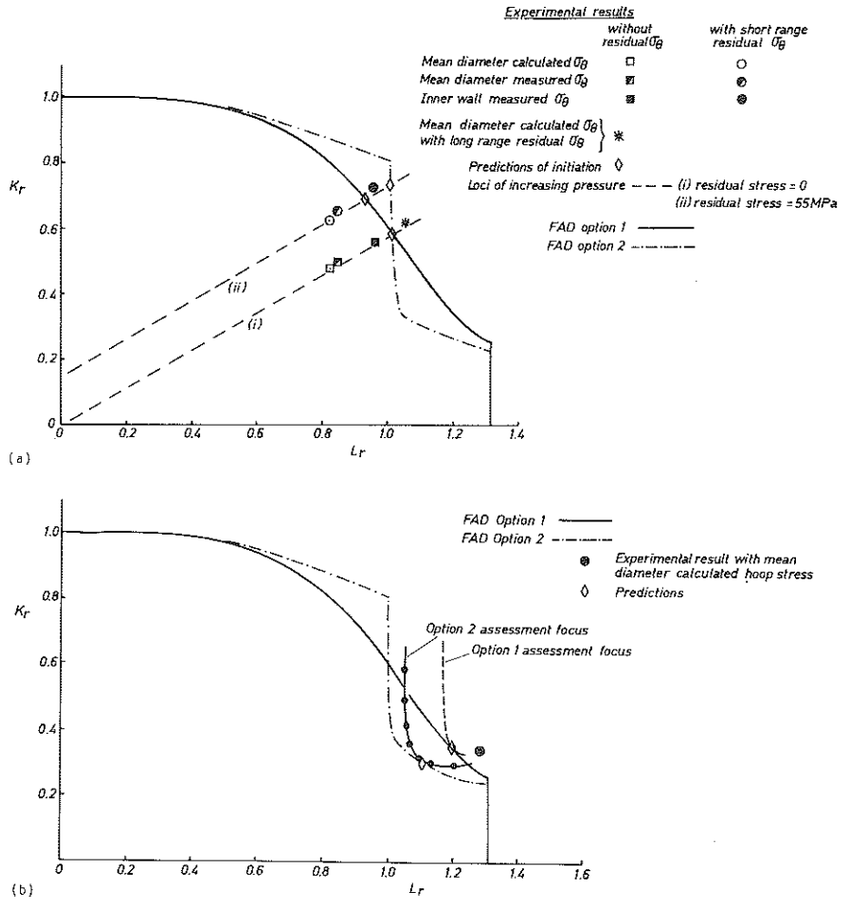

Fig 4 CEGB, R6 revision 3, failure assessment diagram
(a) initiation conditions
(b) failure conditions

mean diameter hoop stress equation (1). For a measured residual stress of 55 MPa, and assuming that this is a short-range residual stress, the locus $[K_r : L_r]$ is parallel to the line for zero residual stress, but with an offset with $K_r^s = 0.15$. For predictions, with and without residual stress, $K_{mat} = 169$ MPa$\sqrt{m}$. The intersection of the line including K_r^s occurs at different $[K_r : L_r]$ points for each option. From Option 1, a lower initiation pressure is predicted than for Option 2.

Also shown in Fig. 4(a) are the $[K_r : L_r]$ points for experimental conditions for initiation at an internal pressure of 11 MPa. The experimental points have been determined for a number of conditions. It can be assumed that there are no residual stresses and K_r and L_r are estimated using:

(a) the mean diameter hoop stress formula, equation (1);
(b) the measured mean hoop stress;
(c) the inner wall surface hoop stresses.

The above can also be repeated for two other cases, namely, assuming that the residual stresses are either short- or long-range. In the former case, the residual stresses contribute to K_r only, while, in the latter, they contribute to K_r and L_r. The predicted pressures for initiation can be compared with experimental conditions in Table 3.

For complete fracture, Fig. 4(b) illustrates the assessment loci for Options 1 and 2. The assessment loci are estimated assuming a constant pressure and zero residual stress. The point of tangency of the assessment loci with the FAD lines gives the predicted instability pressure and the amount of crack extension prior to failure. The results are given in Table 3. Also shown, in Fig. 4(b), is the experimental $[K_r : L_r]$ point corresponding to conditions when the residual stress is zero and using the calculated mean diameter hoop stress, equation (1).

PD 6493 CTOD assessments

The fracture assessment routes proposed for the revised PD6493 follow a three tier approach. In the following, three levels of analyses are presented to determine initiation and fracture instability, respectively, based on the CTOD as a measure of toughness. The normalised toughness parameter $\sqrt{\delta_r}$ is used throughout where

$$\sqrt{\delta_r} = \sqrt{\left(\frac{\delta_I}{\delta_{mat}}\right)} \tag{14}$$

The material toughness δ_{mat} is the measured toughness, as defined below, for the various levels of assessment. δ_I is the crack opening displacement induced at the crack tip. The initiation toughness, $\delta_{0.2}$, was estimated to be 0.15 mm. This initiation toughness was used for all three analysis levels. The maximum load toughness δ_m of the 40 percent side grooved SENB specimens was 0.45 mm at a crack growth of 2 mm. This value is used below to evaluate the failure conditions in the Levels 1 and 2 analyses. For the Level 3 assessment,

Table 3 Prediction of initiation and failure pressures following the CEGB assessment routes

Category	*Predictions*					*Experimental*		
	(1)			(3)				
	Initiation pressure (MPa)		*Crack growth Δa (mm)*	*Instability pressure (MPa)*	*Crack growth Δa (mm)*	*Initiation pressure (MPa) (inferred)*	*Instability pressure (MPa)*	*Average Δa (mm)*
Residual stress (MPa)	0	55		0				
Option								
(1) General curve	13.6	12.8	0.2	15.7	6	~11	16.2	13.2
(2) Reference stress	13.6	13.8	0.2	14.2	10	~11	16.2	13.2

the full CTOD resistance curve up to 12 mm of crack growth is used. As with the R6 assessment, the predictions for the fracture behaviour of the vessel are based on the predicted mean diameter hoop stress, given by equation (1), as well as the measured mean and maximum hoop stresses. Similarly, the Folias correction factor M equation (7) is used.

Level 1 – FAD

The FAD is given by the following equations

$$\begin{aligned} &\sqrt{\delta_r} = 0.707 : 0 \leqslant S_r \leqslant 0.8. \\ &S_r = 0.8 : 0 \leqslant \sqrt{\delta_r} \leqslant 0.707 \end{aligned} \tag{15}$$

The normalised load parameter S_r is defined as

$$S_r = \sigma_n/\sigma_f \tag{16}$$

where σ_n is the effective net section stress given by

$$\sigma_n = \sigma_\theta M \tag{17}$$

The Level 1 FAD is plotted in Fig. 5. The crack opening displacement δ_I induced at the crack tip is given by

$$\begin{aligned} &\delta_I = \frac{K_I^2}{\sigma_Y E}; \quad 0 \leqslant \frac{\sigma_1}{\sigma_Y} \leqslant 0.5 \\ &\delta_I = \frac{K_I^2}{\sigma_Y E}\left(\frac{\sigma_Y}{\sigma_1}\right)^2\left(\frac{\sigma_1}{\sigma_Y} - 0.25\right); \quad 0.5 < \frac{\sigma_1}{\sigma_Y} \end{aligned} \tag{18}$$

where σ_1 is the sum of the maximum of the membrane, bending, peak, and secondary stresses. The locus of increasing applied pressure, based on the calculated hoop stress, for the initiation assessments (i.e., using $\delta_{mat} = \delta_{0.2}$) for residual stresses = 0 and 55 MPa are shown in Fig. 5(a). The predictions for initiation are at the points $[\sqrt{\delta_r} : S_r]$ at which the loci intersect the FAD. The predictions are given in Table 4.

Table 4 Prediction of initiation and failure pressures following the CTOD assessment routes

Condition		*Predictions*					*Experimental*		
		Initiation pressure (MPa)		*Crack growth Δa (mm)*	*Instability pressure (MPa)*	*Crack growth Δa (mm)*	*Initiation pressure (MPa) (inferred)*	*Instability pressure (MPa)*	*Average Δa (mm)*
Residual stress (MPa)		0	55		0				
Model									
Level 1		10.1	7.1	0.2	10.9	2	~11	16.2	13.2
Level 2		12.1	10.2	0.2	16.4	2	~11	16.2	13.2
Level 3	(a)	9.0	7.5	0.2	15.1	4	~11	16.2	13.2
	(b)	9.3	7.5	0.2	14.2	2	~11	16.2	13.2

(a) General curve FAD.
(b) Tensile stress–strain FAD.

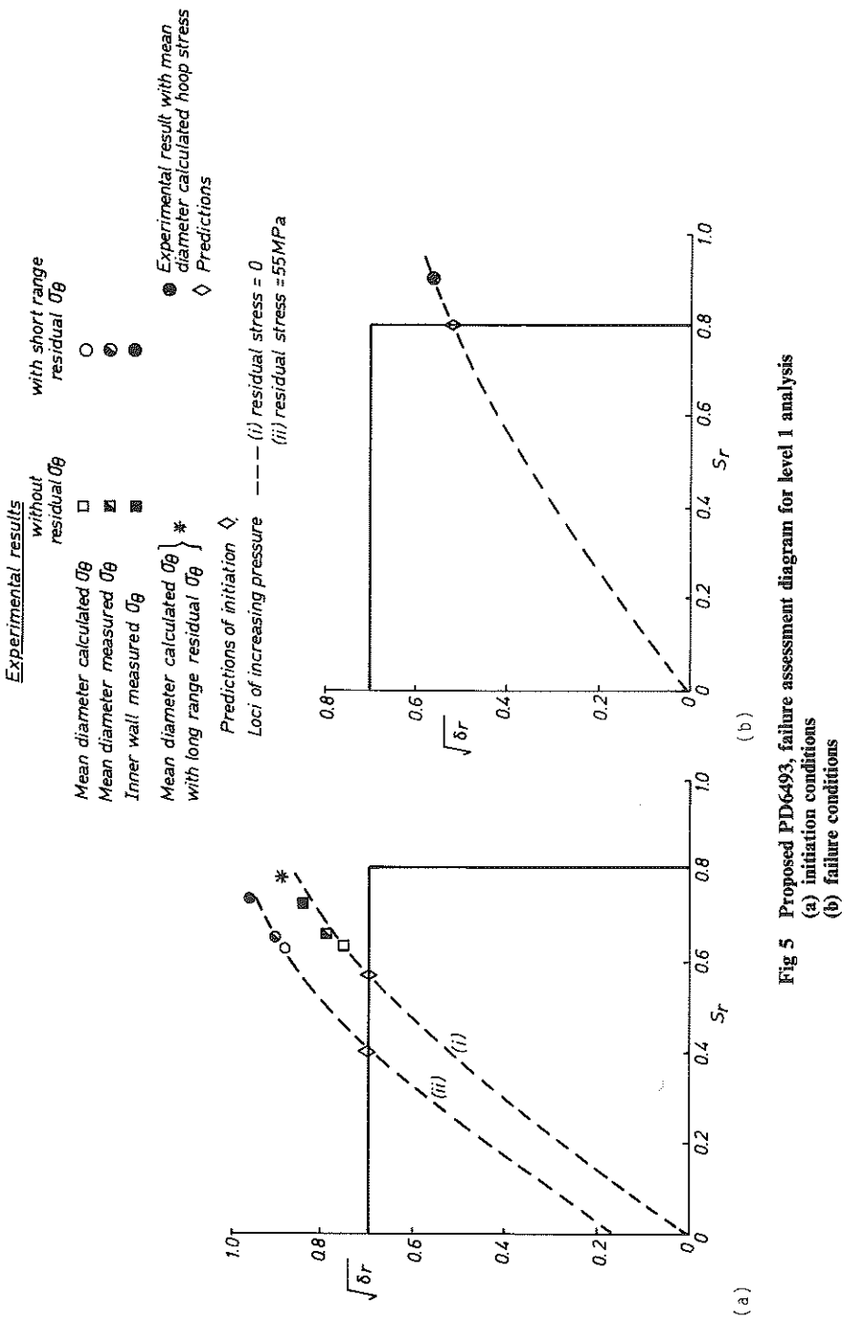

Fig 5 Proposed PD6493, failure assessment diagram for level 1 analysis
(a) initiation conditions
(b) failure conditions

Also shown in Fig. 5(a) are the experimental points $[\sqrt{\delta_r} : S_r]$ for a number of conditions, which were described earlier for the CEGB assessments.

The failure prediction obtained by assuming $\delta_{mat} = \delta_m = 0.45$ mm is shown in Fig. 5(b). The experimental data point $[\sqrt{\delta_r} : S_r]$ is also shown based on the calculated mean diameter hoop stress and no influence of residual stress. A comparison of the predicted and the experiment can be obtained by reference to Table 4.

Level 2 – FAD

The relationship between $\sqrt{\delta_r}$ and S_r in the Level 2 FAD is given by

$$\sqrt{\delta_r} = S_r \left\{ \frac{8}{\pi^2} \ln\sec\left(\frac{\pi}{2} S_r\right) \right\}^{-1/2} \tag{19}$$

where $\sqrt{\delta_r}$ and S_r are given by (14) and (16) respectively. The Level 2 FAD is shown in Fig. 6.

In Level 2 and Level 3 assessments the applied CTOD is given by

$$\delta_I = \frac{K_I^2}{\sigma_Y E} \tag{20}$$

where K_I is the total applied stress intensity factor, given by equation (2).

The normalised toughness parameter, $\sqrt{\delta_r}$, the presence of secondary (residual) stresses is given by

$$\sqrt{\delta_r} = \sqrt{\left(\frac{\delta_I}{\delta_{mat}}\right)} + \rho \tag{21}$$

where ρ takes account of the plasticity interaction effects between secondary and primary stresses.

As in the Level 1 analysis, the FAD has been used to compare predicted and experimental initiation instability pressures, as shown in Fig. 6(a) and (b). The experimental and predicted pressures are given in Table 4.

Level 3 – FAD

There are two options in the proposed Level 3 assessment procedure. In cases where the stress–strain curve may be uncertain, the FAD is described by the FAD given in the R6, Option 1; that is, equation (10) with K_r replaced by $\sqrt{\delta_r}$. The normalised load parameter L_r is given by

$$L_r = \sigma_n/\sigma_Y \tag{22}$$

This FAD is shown in Fig. 7. The locus for increasing applied stress for the initiation assessment is shown in Fig. 7(a). An assessment locus for a given applied pressure and increasing crack length due to tearing is plotted in Fig. 7(b). The point of intersection between the locus and the FAD gives the predicted pressure and the extent of crack growth prior to failure. The second option in the Level 3 assessment is based on the reference stress method and

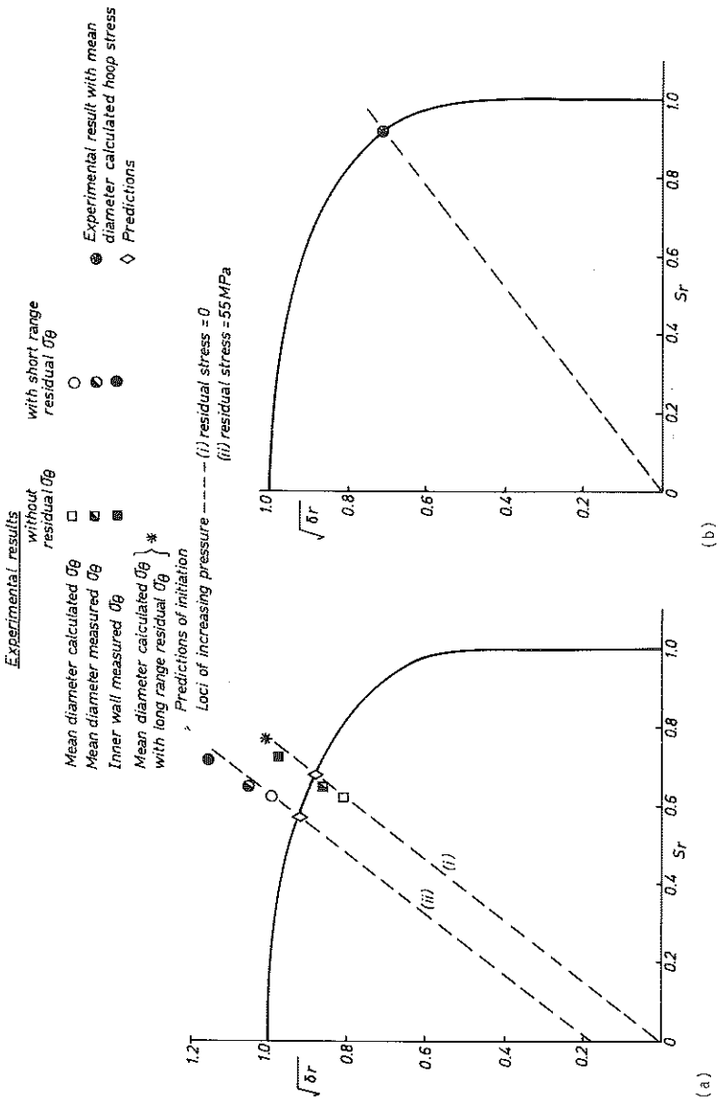

Fig 6 Proposed PD 6493, failure assessment diagram for level 2 analysis
(a) initiation conditions
(b) failure conditions

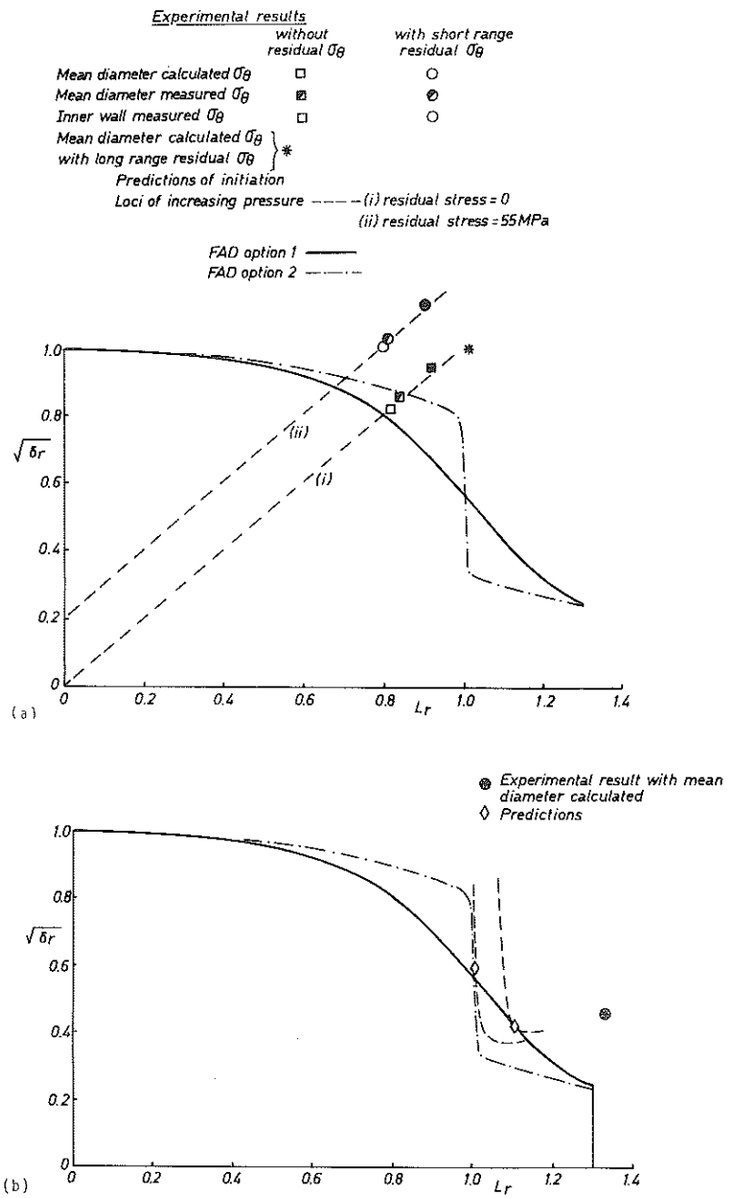

Fig 7 Proposed PD6493, failure assessment diagram for level 3 analysis
(a) initiation conditions
(b) failure conditions

uses the tensile stress–strain curve of the material under examination. The FAD is given by

$$\sqrt{\delta_r} = \left(\frac{E\varepsilon}{\sigma} + \frac{\sigma^3\varepsilon^3}{2\sigma_Y^2 E}\right)^{-1/2} \tag{23}$$

Equation (23) is also plotted in Fig. 7 using the stress strain data given in Table 2. It should be noted that equation (23) reduces to equation (12) where K_r is replaced by $\sqrt{\delta_r}$. The predicted initiation and failure points are shown in Figs 7(a) and (b), respectively, together with the experimental data. Predicted values are given in Table 4.

Discussion

It should be emphasised that even if elastic–plastic plane strain thickness requirements are satisfied, the slope of an R curve is dependent on the geometry of the specimen and, in particular, the mode of loading. The lowest R curves are produced by specimens which experience a large bending component. Consequently, it is normal practice to employ R curves obtained from laboratory bend type specimens, (i.e., SENB or compact) in ductile structural integrity assessments, to increase the degree of conservatism. In this investigation the R curves employed in the assessments were those determined from 40 percent side-grooved SENB specimens which should be significantly lower than the representative R curves for the pressure vessel where the loading was predominantly tensile.

It is evident from Fig. 4(a) and Table 3 that the CEGB R6 assessment route gave a higher initiation pressure than that observed experimentally. Thus, experimental data in terms of $[K_r : L_r]$ based on calculated mean diameter hoop stresses lie within the Options 1 and 2 assessment lines, as shown in Fig. 4. However, it has been shown that the experimentally determined hoop stresses, on the inner wall of the vessel, were significantly higher than were calculated. The maximum inner wall hoop stresses, together with a hoop residual stress of 55 MPa (assumed to be a short-range residual stress) gave an assessment point $[K_r : L_r]$ outside the Option 1 assessment line but inside the Option 2 line. By treating the residual stress of 55 MPa as a long-range residual stress, the experimental assessment point lies outside both Option 1 and Option 2 lines.

In contrast, the prediction of initiation from the Level 1 CTOD assessment route yielded a lower initiation pressure than was observed experimentally. The experimental data for various experimental inputs lie outside the Level 1 assessment line, as shown in Fig. 5(a). The lower prediction, using the Level 1 CTOD assessment, is to be expected since Level 1 has an in-built safety factor on flaw size for linear elastic conditions. In terms of $\sqrt{\delta_r}$, the safety factor is included on the $\sqrt{\delta_r}$ axis with a limit of $1/\sqrt{2}$ (i.e. 0.707).

Turning to the Level 2 and Level 3 CTOD assessments, Figs 6(a) and 7(a) respectively, it can be seen that most experimental inputs provide $[\sqrt{\delta_r} : S_r]$ or $[\sqrt{\delta_r} : L_r]$ points that lie outside the Level 2 and Level 3 assessment line. It is appropriate, therefore, to consider why, on the one hand in the CEGB R6 assessment route experimental data is inside the assessment line while, on the other hand, the same data is outside the CTOD assessment lines.

It is generally accepted that J and δ are related by an expression of the form

$$J = m\sigma_f \delta \tag{24}$$

where m is a constraint factor varying from 1 for tension or predominantly plane stress conditions to 2 for bending or predominantly plane strain conditions. Substituting the experimental values of σ_f, $J_{0.2}$ and $\delta_{0.2}$ for the C–Mn steel gives an m of 2.06. This value is consistent with plane strain conditions for initiation in the 40 percent side grooved SENB specimens.

In using the assessment routes, plane strain values of toughness have been used. For the CEGB R6 route, the applied K conditions have been normalised with respect to bending or plane strain conditions. However, in the CTOD assessment, the applied CTOD, δ_I has been evaluated via the applied K conditions assuming $m = 1$ (i.e., tension loading or plane stress conditions). The applied CTOD is therefore an overestimate for conditions other than tension loading. In practice, it could be argued that a plane stress value of the material toughness, δ_{mat} should be used in the assessment.

It is evident, therefore, that in addition to the inherent factor of safety in the Level 1 CTOD assessment, there is also an additional conservatism in the CTOD assessment routes associated with the evaluation of the applied CTOD.

In the foregoing analyses for complete fracture it has been assumed that the vessel failed by tearing instability whereas, in reality, the final failure mode was cleavage. However, it is quite conceivable that the initial instability failure mode was tearing instability but, as the vessel started to rupture and the local strain rate and/or local constraint increased, the failure mechanism changed to cleavage.

Bearing in mind the above comments, the predictions for instability from Options 1 and 2 of the CEGB R6 route provide lower estimates of instability pressure than was observed. This is illustrated in Fig. 4(b) where the experimental point $[K_r : L_r]$ lies outside the failure assessment line. The prediction from Option 2 is lower than for Option 1.

The predictions for failure in the Level 1 and 2 CTOD assessments are based on maximum load toughness δ_m. In the case of the Level 1 assessment, the experimental point shown in Fig. 5(b) is outside the failure assessment line, so that the predicted failure pressure is lower than observed. In the case of the Level 2 assessment, the experimental point coincides with the prediction. Finally, for the Level 3 assessment, the experimental data point is well outside

the failure assessment lines. The predicted failure pressures are consequently lower than the experimental value.

Concluding remarks

There are a number of features of this test and the application of elastic–plastic defect assessments to predict crack initiation and final failure which cause concern. It appears that there is a potential problem in using nominal formula for accurate and critical predictions. The results from this pressure vessel test have illustrated that significantly higher inner wall hoop stresses can be obtained in a nominally cylindrical thin-walled pressure vessel when compared with calculated hoop stresses. To fully explain the discrepancies between the predicted and observed behaviour in what is considered a simple structural geometry, further large-scale tests are clearly desirable.

The level of residual stresses, after welding in the carbon-manganese steel panel into the pressure vessel, were low at 55 MPa. Nevertheless, their influence in terms of the fracture assessments is significant. In particular, in the case of the CEGB R6 Option 1 assessment, the inclusion of the residual stresses, together with the measured inner wall hoop stresses, provides an assessment point outside the assessment line. In all assessments, by treating the residual stress as a long range or primary stress, the experimental assessment points were outside the assessment lines when using calculated mean diameter hoop stresses.

With the uncertainty in the calculation of hoop stresses using conventional stress formula, together with the uncertainty about the treatment of the measured residual stresses, it appears appropriate that the inherent safety factor of 2 on flaw size incorporated into the Level 1 CTOD assessment may be justified, particularly for initiation conditions. The predictions for complete failure by any of the assessment routes may only be fortuitous, bearing in mind the pressure vessel finally failed by brittle fracture. Nevertheless, all assessment routes and their various options considered in this paper gave failure pressures lower than observed.

Acknowledgements

This work was funded jointly by the Research Members of The Welding Institute, the Minerals and Metals Division of the UK Department of Trade and Industry, and the CEGB. The interpretation of the results and the views expressed in this paper are those of the authors and do not necessarily represent those of the CEGB. We would like to acknowledge the help of Dr Leggatt in the interpretation of the residual stresses, Dr Garwood for his comments on the assessment routes, and Dr Davey for his general comments on the text.

References

(1) BURDEKIN, F. M. and DAWES, M. G. (1971) Practical use of linear elastic and yielding fracture mechanics with particular reference to pressure vessels, *Practical application of fracture mechanics to pressure-vessel technology*, IMechE, London, pp. 28–87.
(2) GORDON, J. R. and GARWOOD, S. J. (1989) A comparison of CTOD ductile instability analyses, *Fracture Mechanics 20th Symposium, ASTM STP 1020*, in press.
(3) GARWOOD, S. J. (1985) A crack tip opening displacement (CTOD) method for the analysis of ductile materials, Welding Institute Research Report 277.
(4) ANDERSON, T. L. (1985) Elastic–plastic fracture assessments based on CTOD, Welding Institute Research Report 276.
(5) HARRISON, R. P., LOOSEMORE, K., and MILNE, I. (1976) Assessment of the integrity of structures containing defects, CEGB Report R/H/R6.
(6) MILNE, I., AINSWORTH, R. A., DOWLING, A. R., and STEWART, A. T. (1986) Assessment of the integrity of structure containing defects, CEGB Report R/H/R6-revision 3.
(7) SMITH, D. J., GREEN, G., and GORDON, J. R. (1988) The testing and the subsequent analysis of a flawed carbon manganese steel pressure vessel, Welding Institute Research Report.
(8) SMITH, D. J. and GORDON, J. R. (1990) Ductile deformation and fracture of a cracked steel pressure vessel, Department of Mechanical Engineering, University of Bristol, Report 90/13.
(9) BEANEY, E. M. and PROCTOR, E. (1974) A critical evaluation of the centre-hole technique for the measurement of residual stresses, *Strain*, **10**, 7–14.
(10) NEALE, B. K., CURRY, D. A., GREEN, G., HAIGH, J. R., and AKHURST, K. N. (1983) A procedure for the determination of the fracture resistance of ductile steels, CEGB Report TPRD/B/0495/84.
(11) GORDON, J. R. (1985) The Welding Institute procedure for the determination of the fracture resistance of fully ductile metals, Welding Institute Research Report 275.
(12) GARWOOD, S. J., GORDON, J. R., WILLOUGHBY, A. A., LEGGATT, R. H., and JUTLA, T. (1988) Crack tip opening displacement (CTOD) methods for fracture assessments: Proposals for revisions to BSI PD6493, Welding Institute Report 371.
(13) AINSWORTH, R. A. (1984) The assessment of defects in structures of strain hardening material, *Engng Fracture Mech.*, **19**, 633.
(14) DUFFY, A. R., McCLURE, G. M., EIBER, R. J., and MAXEY, W. A. (1969) Fracture design practices for pressure piping, *Fracture, an advanced treatise* (Edited by H. Liebowitz), Academic Press, New York, vol. V, ch. 3.